Combustion and Flame 261 (2024) 113292

Contents lists available at ScienceDirect

Combustion and Flame

journal homepage: www.sciencedirect.com/journal/combustion-and-flame

Minimum oxygen supply rate for smouldering propagation: Effect of fuel bulk density and particle size

Yunzhu Qin [a], Yichao Zhang [a], Yuying Chen [a], Shaorun Lin [b,*], Xinyan Huang [a,*]

[a] Research Centre for Fire Safety Engineering, Department of Building Environment and Energy Engineering, The Hong Kong Polytechnic University, Hong Kong SAR
[b] Department of Mechanical Engineering, University of California, Berkeley, CA, United States

ARTICLE INFO

Keywords:
Fuel properties
Smouldering threshold
Propagation pattern
Internal airflow rate
Heat transfer

ABSTRACT

Smouldering is a low-temperature, flameless, and persistent combustion process driven by heterogeneous oxidations. Oxygen supply is a key parameter of smouldering and is sensitive to fuel density and particle size, but our understanding is still limited. Herein, we explore the oxygen threshold for smouldering propagation under upward internal airflow velocities up to 5 mm/s. Pine needles with different bulk densities (55–120 kg/m^3) and wood samples with different particle sizes (1–50 mm) are tested. We found that the minimum airflow velocity for sustaining smouldering propagation increases with the decrease of the bulk density or the increase of the particle size. By increasing the airflow velocity, the smouldering front first propagates unidirectionally (opposed) and then bidirectionally (opposed + forward). Nevertheless, when the pore size is large (the fuel particle size is large or the fuel bulk density is small), bidirectional propagation always occurs, because the oxygen can leak through the opposed smouldering front. A simplified thermochemical analysis is proposed to reveal the influence of interparticle heat transfer on the minimum oxygen supply rate of smouldering propagation. This work advances the fundamental understanding of smouldering on solid fuel particles and their smouldering fire risks and helps optimize the efficiency and safety of smouldering processes.

1. Introduction

Smouldering is a persistent type of combustion that is characterized as a sluggish, low-temperature, and flameless process [1–4]. This heterogeneous phenomenon is sustained by exothermic oxidations when oxygen molecules directly attack the hot surface of condensed-phase reactive porous media [5]. Smouldering combustion includes massive elementary chemical reactions and complex heat and mass transfer processes [6]. Smouldering is notorious for its catastrophic hazards (see Fig. 1a), and it is the primary burning phenomena of residential (e.g., bedding, upholstered furniture and mattresses), industrial (e.g., silos and storage units) and natural (e.g., coal, peat, duff, humus, and wood) fuels [3,7–17]. Nevertheless, smouldering has also been utilized for energy conversion and adopted as an effective alternative to conventional organic waste removal technology, showing promising application prospects [18,19]. Thus, a better understanding of the smouldering process may not only help prevent undesirable fire accidents but also optimize the efficiency and safety of applied smouldering systems [4,20].

The propagation and extinction of smouldering combustion are primarily controlled by two key mechanisms: heat loss and oxygen supply [2,3,22,23]. The path and rate of oxygen supply are crucial for the heterogeneous oxidations that generate the required heat to balance endothermic processes such as drying, pre-heating, environmental cooling, and endothermic pyrolysis reactions during propagation [21]. However, smouldering combustion is an incomplete reaction process requiring less oxygen for a self-sustaining front than flaming combustion, leading to a lower limiting oxygen concentration (LOC) [21,24]. Therefore, smouldering of porous fuels can be initiated and sustained with a limited oxygen supply, e.g., the deep underground peat and coal fires [25,26].

However, past research on the oxygen supply limits of smouldering has been mainly conducted under quiescent ambient or with external wind, which cannot completely separate the diffusion of oxygen from the surroundings [21]. This has resulted in different values of limiting oxygen concentration (LOC) found for the same fuel in various experiments [27–29], and the actual minimum rate of oxygen needed to sustain smouldering is still unclear. Therefore, to quantify the LOC for smouldering propagation, it is necessary to accurately measure the amount of oxygen passing through the porous fuel.

In our previous work [21], we developed a tubular smouldering

* Corresponding authors.
E-mail addresses: shaorun.lin@berkeley.edu (S. Lin), xy.huang@polyu.edu.hk (X. Huang).

https://doi.org/10.1016/j.combustflame.2024.113292
Received 21 June 2023; Received in revised form 1 January 2024; Accepted 2 January 2024
Available online 13 January 2024

Nomenclature

Symbols

A_c	cross-section area (m^2)
d	fuel diameter (mm)
d_p	characteristic pore size (m)
ΔH	heat of reaction (MJ/kg)
k	effective thermal conductivity (W/m·K)
L	fuel length (mm)
m	mass flow rate (g/s)
$\dot{m}''$	mass flux (g/m^2·s)
n_k	reaction order (-)
$\dot{q}''$	heat flux (kW/m^2)
S	particle surface area (m^2/g)
T	temperature (°C)
U	flow velocity (mm/s)
Δx	characteristic length (m)
X	volume fraction (-)
Y	mass fraction (-)

Greeks

β	heating rate (K/min)
γ	radiative conductivity coefficient (m)
ρ_b	bulk density (kg/m^3)
ρ_g	gas density (kg/m^3)
ρ_s	solid density (kg/m^3)
σ	Stefan–Boltzmann constant ($(kg/s^3 \cdot K^4)$)
ψ	porosity (-)

Subscripts

cond	conduction
conv	convection
g	gas
min	minimum
O_2	oxygen
ox	oxidation or oxidizer
r	radiative
sm	smouldering
0	initial

Abbreviations

LOC	Limiting oxygen concentration
TG	Thermogravimetric

reactor that could flow the oxidizer through the porous fuel to the smouldering front without an ambient oxygen supply. We found that, for peat soil with high organic content, the LOC could be below 2 %, and the minimum internal oxygen supply rate was approximately 0.08 ± 0.01 g/m^2·s. Such a minimum value was almost a constant when the oxygen mass fraction (Y_{O_2}) was larger than 15 % (see Fig. 1(b)). However, the LOC and minimum internal oxygen supply rate of common fuels, such as wood [18,20,30], coal [31], and biowastes [32,33], are still unclear. Furthermore, even for a particular kind of fuel, its properties such as particle size, bulk density and moisture content may also affect the thresholds of smouldering propagation. Therefore, we need to further understand the oxygen-supply threshold of smouldering ignition and propagation [34], as well as how underlying physical and chemical mechanisms change with the fuel parameters at near-limit conditions.

This study aims to explore the role of fuel size and bulk density on the minimum oxygen supply rate of smouldering combustion. Wood and pine needles are selected as representative porous fuel beds to support a robust smouldering propagation. Controlled airflow (X_{O_2} = 21 %) is provided to penetrate through the porous fuel bed with a velocity of up to 5 mm/s inside the smouldering reactor. The evolutions of fuel smouldering mass loss and temperature profile are quantified under different internal oxygen supply rates. Finally, a heat transfer analysis is proposed to explain the influence of fuel particle size and bulk density on the minimum oxygen supply rate of smouldering.

2. Experimental method

2.1. Fuel samples and processing

Wood and pine needles, as typical porous fuels that are prone to smouldering combustion [18,35,36], were tested in this work (Fig. 2a). Although duff and peat were also viable options for the experiment, they either exhibited a complex mixture composition or posed challenges in adjusting bulk density through compression. Consequently, we have opted for wood samples and pine needles as they effectively meet the experimental requirements. The large wood chips with homogenous physical properties were provided by a local supplier (ECO-Greentech Ltd.), while the pine needles were collected from the larch forest in Saihanwula Biosphere Reserve, China. Thermogravimetric tests were conducted using PerkinElmer STA6000 under air and N_2 atmospheres, and representative results are shown in Fig. S1.

Before being placed into the smouldering reactor (Fig. 2b), all the fuel samples were oven-dried at 90 °C for at least 48 h. Then, the final moisture content of dry fuel was measured to be < 5 %, which is low

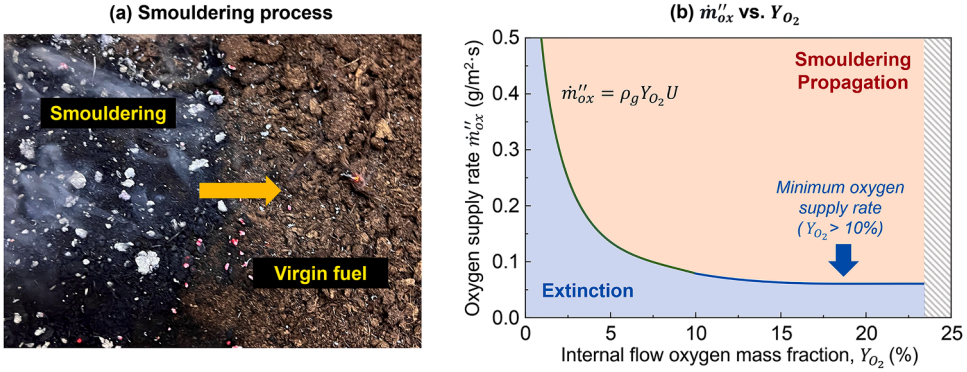

Fig. 1. (a) Smouldering, the flameless combustion, in organic peat soil. (b) minimum oxygen mass flow rate for supporting smouldering in peat at different oxygen mass fraction [21], where the oxygen limit reaches a minimum value of 0.08 ± 0.01 g/m^2·s when Y_{O_2} > 15 %.

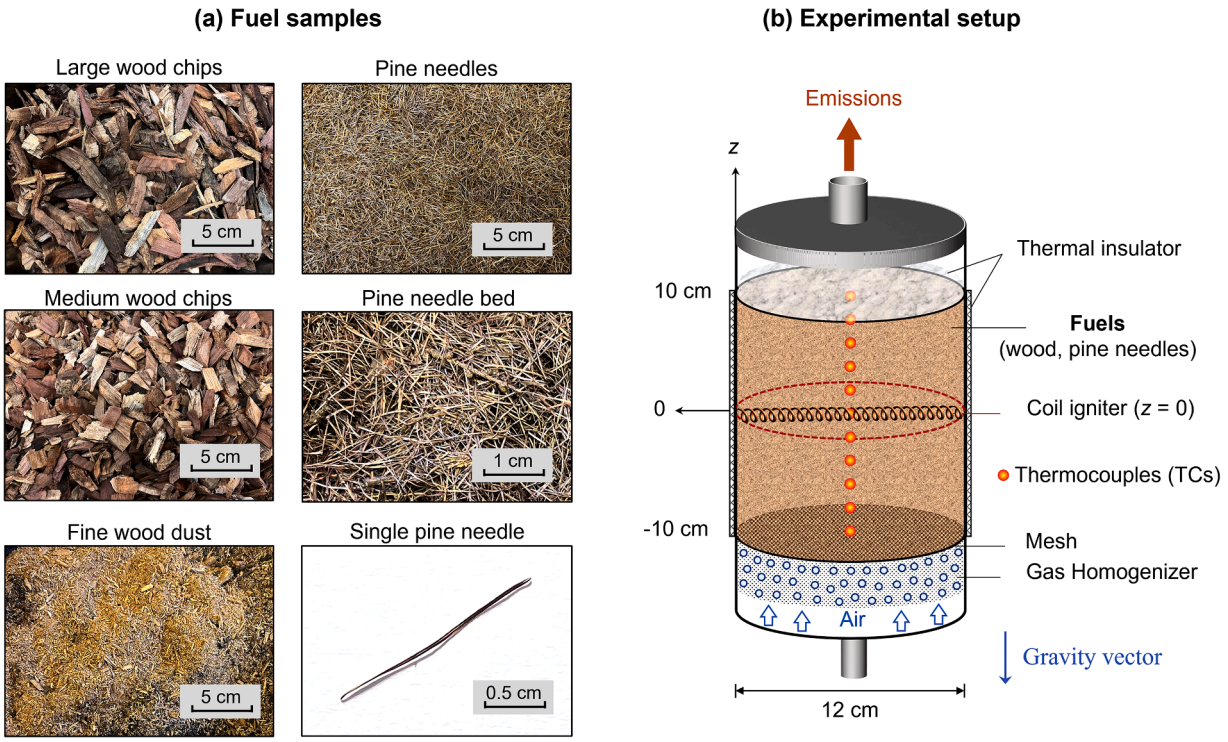

Fig. 2. (a) Tested samples of wood (large, medium chips and fine dust) and pine needles (in different observation views) and (b) schematic diagram of the experimental setup.

enough not to affect the smouldering propagation [27,37]. In general, wood chips were relatively stiff, and it was more feasible to control the fuel size. Comparatively, pine needles were relatively loose, and it was easier to change the bulk density. Thus, two groups of experiments were designed:

(I) woods with three particle sizes (d) of 1 (fine dust), 25 (medium), 50 mm (large), and
(II) pine needles with the same size (diameter (d) of 0.2 mm and length (L) of 25 mm) but three bulk densities of 55, 80, and 120 kg/m^3.

Note that the bulk densities (ρ_b) of medium (162 ± 20 kg/m^3) and large chips (178 ± 30 kg/m^3) were close to each other, while the bulk density of fine wood dust (325 ± 20 kg/m^3) doubled. A larger measurement error in bulk density is attributed to the strong dependency on stacking situation (e.g., the direction of chips), particularly in cases where particle size is relatively large. Since the solid density (ρ_s) of the wood material was about 600 kg/m^3 [18], the porosities ($\psi = 1 - \rho_b/\rho_s$) of the large, medium, and fine wood samples were 0.7 ± 0.02, 0.73 ± 0.03 and 0.46 ± 0.03, respectively. The physicochemical properties of fuel samples in the experiments are summarized in Table. 1. Fig. 3 plots the relationship between fuel particle size and fuel-bed bulk density.

2.2. Experimental setup and procedure

The smouldering experiments were conducted in a tubular smouldering reactor (vertical) with an ignition system and an air supply system, as detailed in Fig. 2b. The tubular reactor was made of 2-mm thick quartz glass and had a total depth of 35 cm, updated from the previous work [21]. The internal diameter of the reactor was designed to be 12 cm with a cross-section area of $A_c = 113$ cm^2, which is large enough to minimize the effect of lateral wall cooling [38,39].

The purified air with a maximum internal flow velocity of 5 mm/s was pushed into the porous fuel bed from the bottom. Considering that gravity and buoyancy can potentially affect smouldering extinction limits [40], the results may vary depending on the direction of the oxygen supply. Note that in this work the internal flow velocity was an overall value for the cross-section of the reactor ($U = m/\rho_g A_c$), not a local velocity inside small pores. A sandwiched gas homogenizer (mesh + 5-cm layer of glass beads + mesh) was placed at the bottom of the reactor to create a relatively uniform air supply. Above the homogenizer, a fresh fuel sample layer with a constant height of 20 cm was added to the reactor.

To further reduce the influence of environmental cooling on the smouldering process, a 1-cm thick thermal insulation layer was placed on top of the fuel and attached to the outer surface of the reactor. To monitor the smouldering process, an array of eleven K-type

Table 1
Properties of dry fuel samples in the experiments.

Fuel	Particle size d (mm)	Bulk density ρ_b (kg/m^3)	Solid density ρ_s (kg/m^3)	Porosity ψ (-)	Volatile (%)	Fix carbon (%)	Ash (%)
Wood	1 ± 0.5 (Fine) 25 ± 5 (medium) 50 ± 10 (large)	325 ± 20 162 ± 20 178 ± 30	600 ± 20	0.46 ± 0.03 0.73 ± 0.03 0.70 ± 0.02	58.8	38.9	1.1
Pine needles	d = 0.2 ± 0.1 L = 25 ± 5	55 ± 5 80 ± 10 120 ± 15	607 ± 30	0.91 ± 0.01 0.87 ± 0.02 0.80 ± 0.02	47.1	35.7	14.3

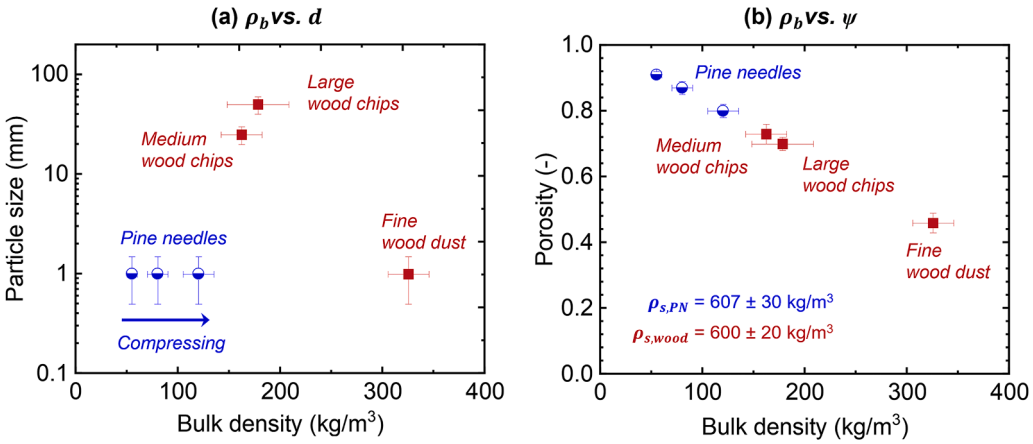

Fig. 3. Bulk density versus (a) fuel size and (b) fuel bed porosity of tested pine needles and wood samples.

thermocouples (1 mm bead diameter) was inserted into the fuel with an interval of 2 cm, recording the temperature profiles in 1-min time intervals for the whole experimental process. The coil ignitor was inserted into the middle of the sample ($z = 0$) to initiate the smouldering combustion. The ignition protocol was fixed at 100 W for 20 min, which was strong enough to ignite the tested dry fuel samples. After the ignition stage, the ignitor was switched off and then the forced internal airflow was fed into the fuel bed.

During the tests, the holes for inserting coil ignitor and thermocouples were well sealed. To ensure that oxygen was only provided from bottom-supplied airflow controlled by a precise flow meter (measured uncertainty $< \pm 5$ %), a gas outlet with a diameter narrowed to 1 cm was set on the top of the reactor to enable the release of emission gas and prevent atmospheric oxygen from entering the reacting sample [21]. During all lab experiments, the ambient temperature was 25 ± 3 °C, the relative humidity was 50 ± 20 % (equivalently 1.5 ± 0.6 % mole fraction of water in the air), and the pressure was 101 kPa. At least three replicates were conducted for each scenario. If three repeated experiments have the same results (propagation or extinction), the experimental repeatability can be ensured, similar to our previous work [21, 38].

3. Results and discussion

3.1. Smouldering propagation phenomena

Fig. 4 shows the thermocouple measurements of medium wood chips under different internal airflow velocities. In general, as the airflow supply rate decreases, the fire-propagation mode changes from (a) bidirectional propagation to (b) unidirectional propagation to (c) no propagation. Similar trends were also observed for wood dust and pine needles in this work and for organic soil in our previous work [21].

Under an internal airflow of 4.4 mm/s (Fig. 4a), by the end of ignition, the thermocouple reading near the coil ignition was higher than 300 °C, thus a smouldering reaction zone was formed. Then, the coil heating was interrupted, and the purified air with the prescribed flow velocity was provided. Afterwards, two separated (forward and opposed) smouldering fronts were observed under this single forced airflow, evidenced by the temperatures over 300 °C both above ($z > 0$) and below ($z < 0$) the ignition zone. At a relatively high flow velocity, the supplied oxygen was partially consumed by the downward (opposed) front, and the remaining oxygen escaped and then played a role in supporting the upward (forward) front. As a result, the opposed front usually has a higher smouldering temperature (observed by thermocouple data) and a more complete combustion process (residual evidence of more ash on the bottom) than that of the forward front. The heat transfer process that affects peak smouldering temperature will be analysed in Section 3.5.

When the airflow rate was decreased to 1.5 mm/s (Fig. 4b), with the same ignition protocol and air-supply timing in this scenario, only an opposed smouldering front was sustained (> 250 °C) because of the limited oxygen provided. The offered oxygen was fully consumed by the downward smouldering front. Note that the thermocouple reading at 6 cm is higher than that at 2 cm during ignition. This abnormal phenomenon is potentially because of (1) a non-uniform reaction front under an oxygen-limited condition; (2) the probe of the thermocouple point at 2 cm may not fully touch the fuel. After burnout, the fuel surface was found to regress significantly, and a clear boundary can also be observed with virgin fuel above and ash and unburned char below.

Gradually reducing the oxygen supply, it was found that when the airflow was small enough, the oxygen supplied was unable to support smouldering propagation, as shown in Fig. 4c. To be specific, the temperature in the entire reactor is rapidly reduced to room temperature without any fluctuation after the ignition. Further prolonging the heating duration or increasing the heating power still cannot induce the smouldering propagation at this oxygen supply rate.

3.2. Smouldering oxygen supply limits vs. fuel-bed bulk density

Fig. 5 plots the internal airflow velocity vs. (a) bulk density (ρ_b) and (b) porosity (ψ) of pine-needle beds and shows the smouldering phenomena under different scenarios. Three smouldering phenomena of "bidirectional propagation", "unidirectional propagation", and "no propagation" define two oxygen supply boundaries. On one hand, Fig. 5a shows the minimum oxygen supply decreases with the fuel dry bulk density, that is, fuels with higher bulk densities require less oxygen to support a smouldering propagation. Specifically, when the bulk density was increased from 55 kg/m^3 to 120 kg/m^3, the U_{min} decreased significantly from 0.5 mm/s to 0.2 mm/s.

On the other hand, the boundary between bidirectional and unidirectional propagation shows an opposite trend. In other words, pine needles with higher bulk densities are more prone to unidirectional propagation within the tested range. For the pine needles with a bulk density of 120 kg/m^3, bidirectional propagation in the vertical direction can only be observed at a larger airflow velocity (near 3 mm/s). In contrast, for pine needles close to their natural bulk density (~45 kg/m^3), as long as the provided airflow is larger than the minimum supply limit, both upward and downward smouldering fronts can be formed and sustained. The reason behind this "bidirectional smouldering propagation" is not the excessive O_2 supply to a uniform front (as illustrated in Fig. 6a and detailed in our previous work [21]). In contrast, Fig. 6b illustrates two more scenarios that lead to bidirectional smouldering by leaked oxygen (B1: due to high-porosity fuel bed; B2: due to large particles). When the particles are loosely packed, the "leaked

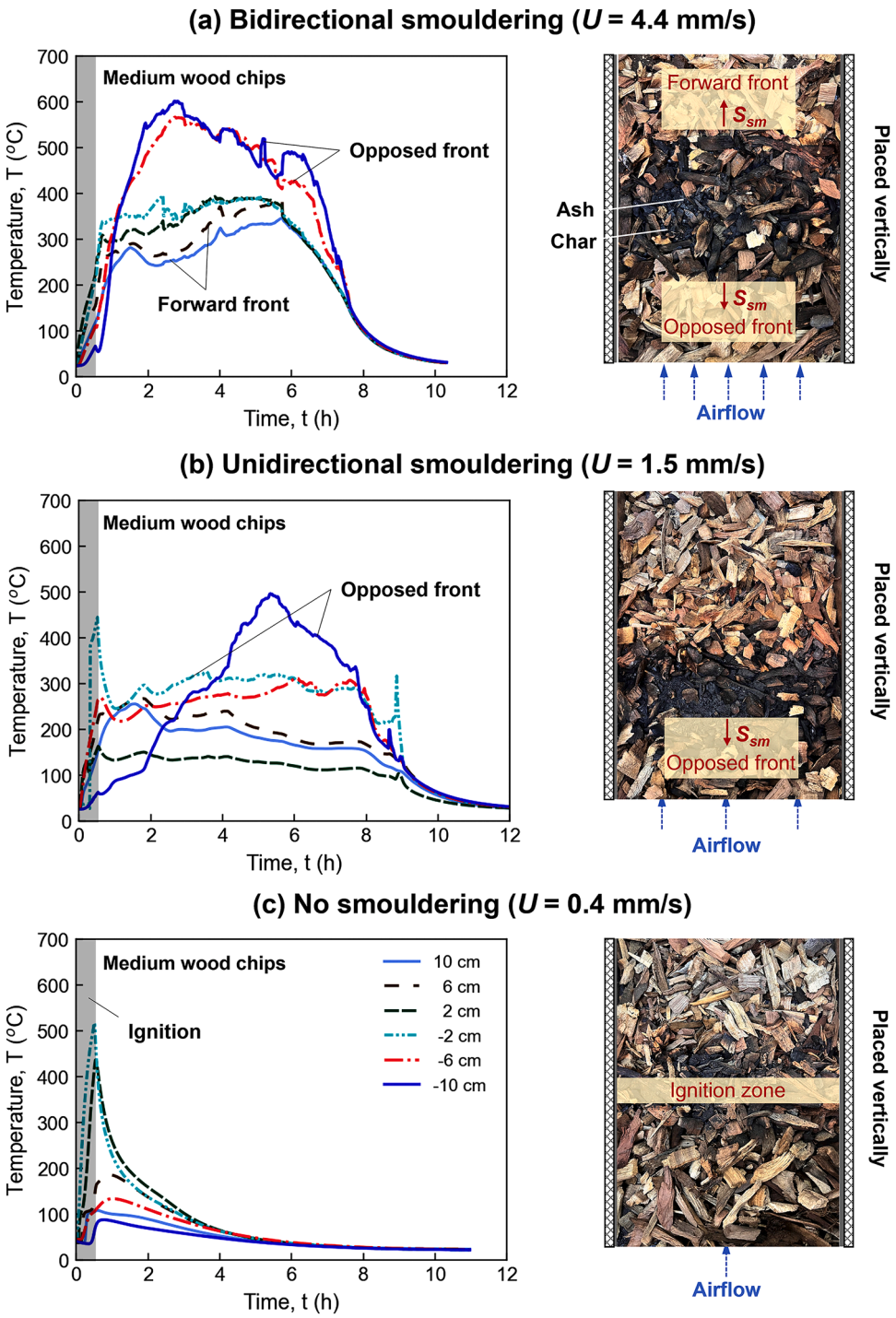

Fig. 4. Thermocouple measurements and schematic diagrams of (a) bidirectional smouldering, (b) unidirectional smouldering and (c) no smouldering (extinction after ignition) in medium-size wood chips with internal airflow supply rate of 4.4 mm/s, 1.5 mm/s and 0.4 mm/s, respectively.

oxidizer" through the pores between the particles will lead to a non-uniform smouldering front in the higher-porous fuels. Therefore, it is easier to sustain the bidirectional propagation for fuel beds with a lower bulk density (see Fig. 6b (B1)).

Fig. 5(c-d) further summarizes experimental data on minimum flow velocity U_{min} to sustain smouldering combustion in fuels with different fuel porosities but with similar particle sizes (0.5~2 mm), including pine needles, wood dust, and peat soil [21]. While there are still differences in other physical properties of fuels, organic content, and heat of combustion (see Table 1 and Supplemental Materials), the results indicate that in the premise of comparable particle sizes, bulk density plays one of the determinant roles in controlling the minimum oxygen requirements of smouldering combustion in diverse fuels. More experimental data from diverse fuels and theoretical work are needed to evaluate the role and contribution of each parameter.

3.3. Smouldering oxygen supply limits vs. fuel particle size

Based on the experimental results, the effect of density on the U_{min} can also be applied to wood samples to some extent, as shown in Fig. 7a. In general, wood samples with higher bulk densities require less oxygen to support unidirectional smouldering combustion, but a larger flow rate

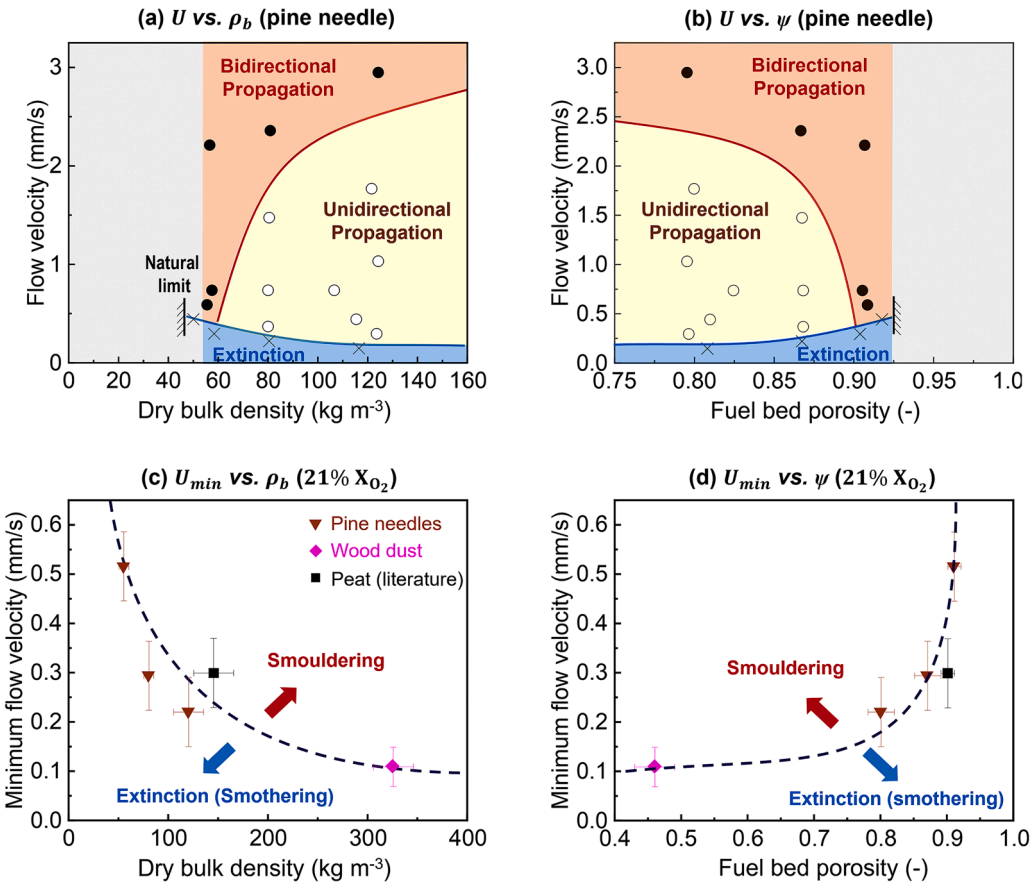

Fig. 5. Internal airflow velocity vs. (a) pine needle bulk density and (b) porosity, where ●: bidirectional, ○: unidirectional, and ×: extinction. Minimum internal airflow velocity vs. (c) fuel bulk density and (d) porosity for different fuel beds.

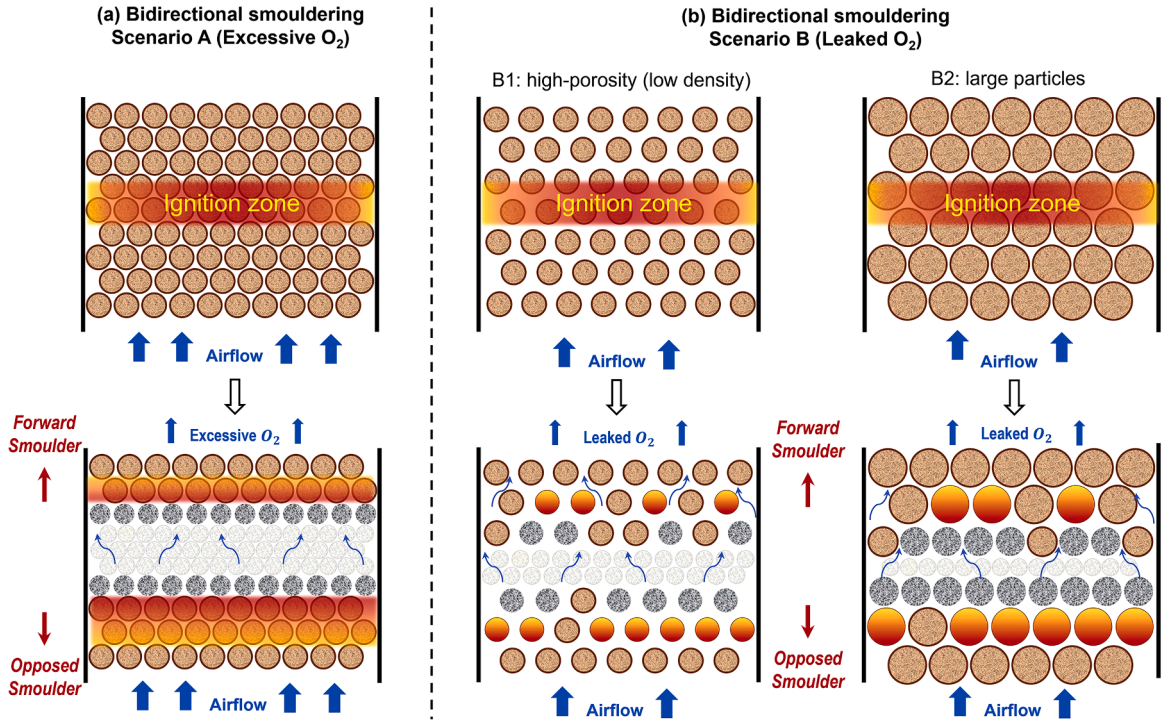

Fig. 6. Two scenarios of bidirectional smouldering propagation, (a) excessive oxygen not fully consumed by the opposed front; and (b) leaked oxygen due to B1: high-porosity (low-density) fuel bed or B2: large fuel particles.

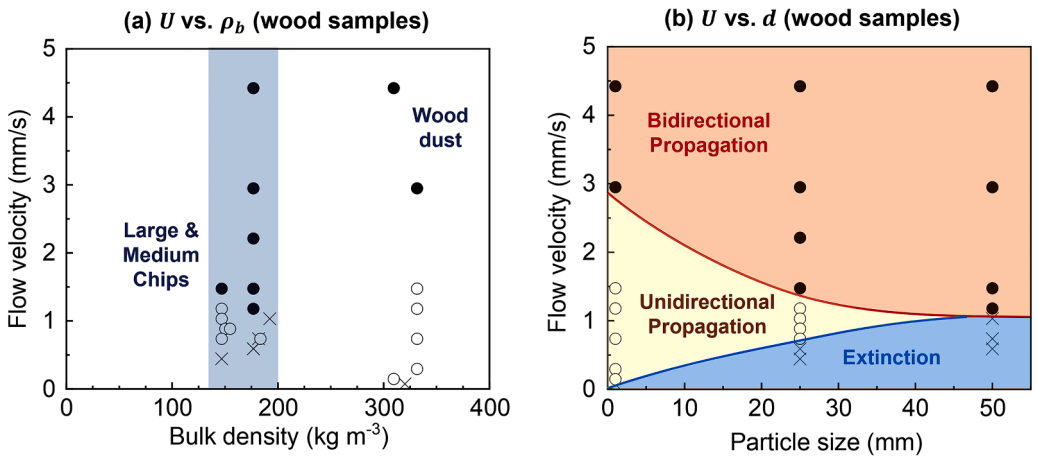

Fig. 7. Internal airflow velocity vs. (a) dry bulk density and (b) particle size of wood samples, where ●, ○, and × represent "bidirectional propagation", "unidirectional propagation" and "no propagation", respectively.

for bidirectional propagation. However, an anomaly was found when focusing on bulk density between 150 and 200 kg/m^3, that is, the relationship between ρ_b and U_{min} is unclear in this small range. This is because even though large and medium wood chips have a distinguishable difference in particle size, their bulk density is highly dependent on the stacking situation, e.g., the direction of chips, thus inducing a strong random impact on local bulk density (ρ_b). Therefore, in terms of wood samples, the experimental results were reformatted as a relationship between particle size and flow velocity.

Fig. 7b summarizes the experimental results of the minimum airflow rate to support the smouldering combustion of wood samples with different particle sizes. It shows that the effect of reducing particle size is similar to that of increasing bulk density, that is, samples with a lower particle size have a lower limit of U_{min} to support smouldering

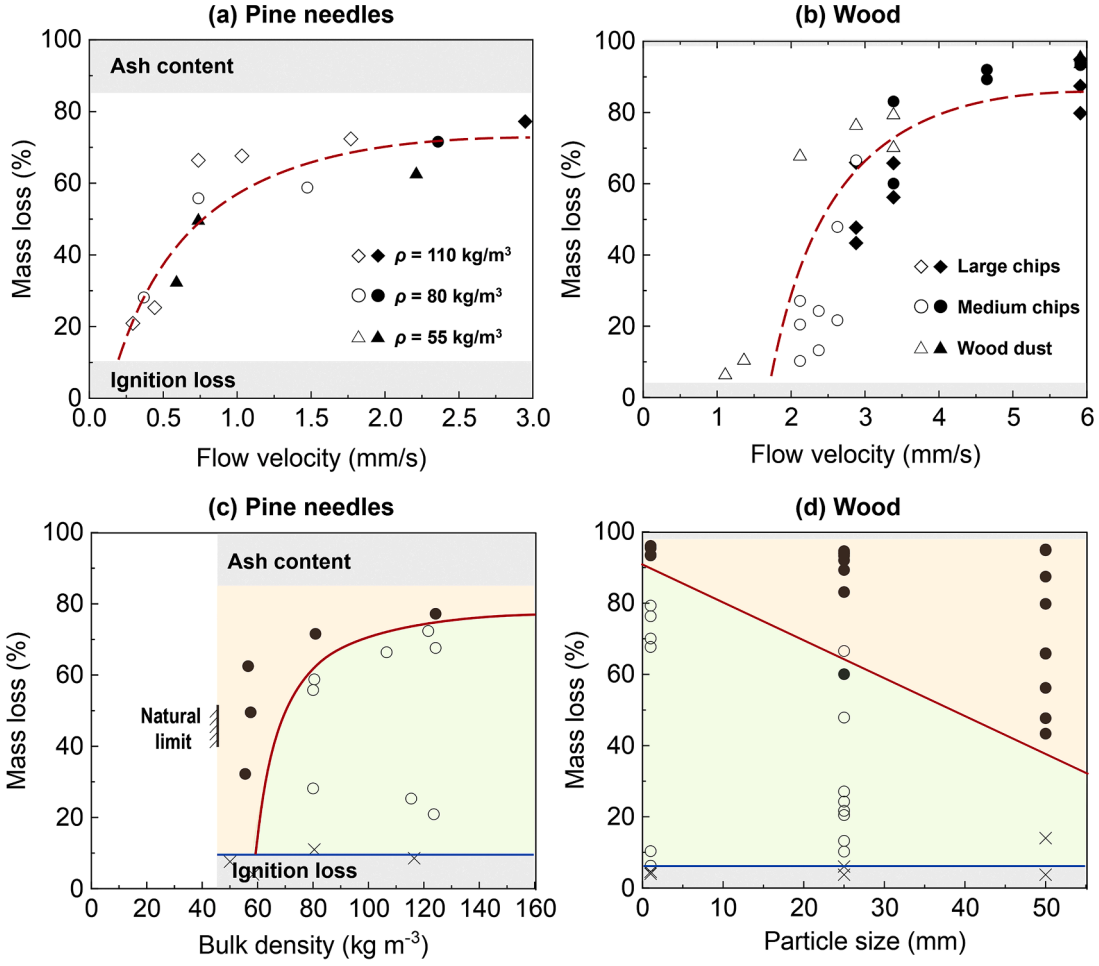

Fig. 8. The effect of (a-b) internal airflow velocity, (c) bulk density and (d) particle size on mass loss during smouldering, where ○ is unidirectional propagation, and ● is bidirectional propagation.

combustion. However, only bidirectional propagation was found in large wood chips ($d = 50$ mm) when the airflow velocity was larger than 1 mm/s.

Similarly, the enlarged particle size can also induce non-uniform smouldering propagation. Thus, the leaked O_2 can result in the forward propagation front (Fig. 6b (B2) and Fig. 7b). This explains bidirectional smouldering propagation in large fuel particle sizes with relatively low airflow velocities.

3.4. Smouldering mass loss and temperature

Mass loss and peak temperature are critical smouldering characteristics to reveal their underlying mechanism in the near-limit condition. Fig. 8 summarizes the overall burning mass loss after the smouldering process, where hollow and solid symbols represent uni- and bidirectional propagation, respectively. All the data were obtained by varying airflow velocity in individual tests. First of all, the ignition process led to higher mass loss in pine needles than in wood samples. However, the overall burning mass loss of pine needles is lower than wood samples in high flow velocities, due to a higher proportion of ash content (determined by the TG test, see Table 1 and Supplemental Materials).

Nevertheless, the smouldering mass loss for both wood and pine needles increases with the internal airflow rate, regardless of particle size, bulk density and propagation mode. This implies the importance of controlling oxygen supply in smouldering biomass removal systems [18,20,41]. It is worth noting that, bidirectional propagation does not necessarily cause greater mass loss than unidirectional propagation. In other words, no universal boundary between uni- and bidirectional propagation was found, and mass loss cannot be used as direct evidence to determine the propagation mode, but instead has to be in conjunction with the temperature distribution. Similar phenomena can also be observed in wood samples (Fig. 8b). Moreover, Fig. 8(c-d) provides a comparison of the effect of bulk density and particle size on burning mass loss. It suggests that the bidirectional propagation results from low bulk density or high particle size led to lower mass loss during smouldering combustion.

Fig. 9 summarizes the peak smouldering temperature during the combustion process in both fuels. Note that it refers to the average peak temperature of the front in the unidirectional propagation, or the average temperature of both fronts in the bidirectional propagation of repeating tests, and the standard deviations are shown as error bars. As expected, peak smouldering temperature increases with the supplied oxidizer flow, due to better oxygen availability and thus more heat released from the char oxidation process. This also explains the trend of mass loss change with flow velocity in Fig. 8.

Similarly, peak smouldering temperature cannot be applied as a criterion to distinguish the propagation mode. For example, in large wood samples with an airflow velocity of 1.2 mm/s, bidirectional propagation with low peak temperature was observed (see Fig. 8b). This provides another possibility for the bidirectional propagation smouldering, i.e., in addition to the excess oxygen that cannot be completely consumed by a single front [21], it may also be due to the oxygen "leakage" from the non-uniform smouldering front, as a result of low bulk density or large fuel particle size (see Fig. 6).

Furthermore, pine needles are also found to have a slightly higher minimum smouldering temperature (~300 °C) than wood samples (~250 °C). Although the trend of the peak temperature with the changing

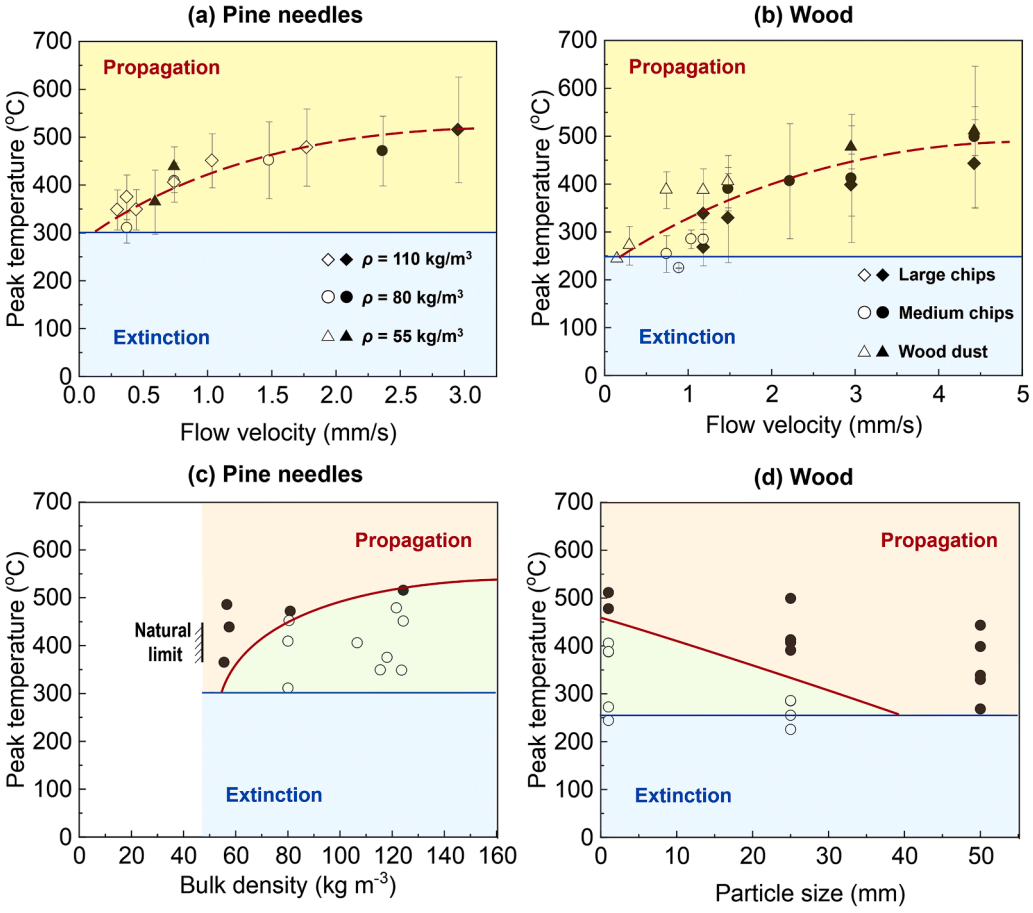

Fig. 9. The effect of (a-b) flow velocity, (c) bulk density and (d) particle size on peak smouldering temperatures, where the hollow (○) and solid (●) symbols represent uni- and bi-directional propagation, respectively.

oxygen supply is similar, the variation of bulk density and particle size variations didn't substantially affect peak temperature under similar oxygen supply conditions (see Fig. 9(a-b)). In addition, Fig. 9(c-d) provides a further comparison of the influence of bulk density and particle size on the peak temperature. It indicates that bidirectional propagation under low bulk density or high particle size led to lower peak smouldering temperatures.

3.5. Heat and mass transfer analysis

Basically, the self-sustained smouldering process is thermally controlled by three heat transport mechanisms, i.e., conduction, convection and radiation. Based on the law of energy conservation, an approximate and simplified heat transfer analysis can be applied to the smouldering front at the near-limit condition (Fig. 10). At the propagation or extinction limit, the net heat released from the smouldering front ($\dot{q}''_{sm}$) should just overcome the heat loss ($\dot{q}''_{loss}$) as

$$\dot{q}''_{sm} \geq \dot{q}''_{loss} \tag{1}$$

As smouldering propagation is primarily controlled by thermal conduction in this porous fuel system with a low-velocity forced airflow (<1 mm/s) [42], by rearranging Eq. (1), we obtain

$$\dot{q}''_{sm} = \dot{m}''_{O_2,\min}\Delta H_{ox} = \rho_g U_{\min} Y_{O_2}\Delta H_{ox} \approx \dot{q}''_{cond} = k\frac{(T_{sm}-T_0)}{\Delta x} \tag{2}$$

where k is the effective thermal conductivity in porous media (as a solid-fluid system), T_{sm} is the smouldering temperature, T_0 is the temperature of virgin fuel, Δx is the characteristic length of conductive heat transfer. Therefore, the minimum flow velocity U_{min} can be derived as

$$U_{min} = \frac{k(T_{sm}-T_0)}{\rho_g Y_{O_2}\Delta H_{ox}\Delta x} \tag{3}$$

Furthermore, the effective thermal conductivity k includes a solid (k_s) and a radiative (k_r) component, and the latter is attributed to radiation heat transfer across pores and becomes a dominant mode of heat transfer in porous media during smouldering combustion [43], thus

$$k = k_s(T) + k_r(T) \approx \left(\psi k_g + (1-\psi)k_0\right)\left(\frac{T}{T_r}\right)^{n_k} + \gamma\sigma T^3 \approx \gamma\sigma T^3 \tag{4}$$

where n_k is the temperature dependence, σ is the Stefan-Boltzmann constant, γ is the radiative conductivity parameter (with units of length) that depends on pore morphology and other considerations and can be estimated by characterized pore size d_p as $\gamma = 3d_p$ [44,45]. The characterized pore size relates to the particle surface area (S, m^2/g) and bulk density (ρ_b, kg/m^3) as $d_p = 1/S\rho_b$ [44]. Therefore, from Eqs. (3-4), as the bulk density of fuel increases, d_p, γ and k will decrease accordingly, leading to a lower minimum flow velocity (U_{min}) as

$$U_{min} \sim k \sim \gamma \propto d_p \propto \frac{1}{\rho} \tag{5}$$

On the other hand, as the particle size (d) increases, the specific surface area (S) will decrease and the characterized pore size (d_p) will increase. As a result, both γ and k will increase simultaneously, leading to a larger minimum flow velocity (U_{min}) as

$$U_{min} \sim k \sim \gamma \propto d_p \propto \frac{1}{S} \propto d \tag{6}$$

In other words, increased fuel bulk densities or smaller fuel particle sizes can both lower the minimum oxygen supply required for smouldering propagation by enhancing heat conduction between the burning zone and virgin fuels. Thus, the proposed heat transfer analysis successfully explains the experimental data (Fig. 5a and 7b) and indicates the important role of radiation heat transfer across pores in affecting the oxygen supply limit of smouldering propagation over porous media. Note that this theoretical analysis has constant solid density approximation which is applied for single component fuel (pine needles or wood chips). However, when the fuel becomes a mixture of solid fuels, this analysis may not be appropriate because of varying solid density ρ_s in the system. Further investigations are required to elucidate the role of complex fuel properties of solid mixtures.

Even though the experiments and analysis revealed the role of fuel bulk density and particle size in the minimum oxygen supply for smouldering, further experimental and simulation studies are needed to establish the relationship between U_{min} and other fuel characteristics, such as moisture content, organic content, and heat of combustion. These efforts will not only advance our understanding of smouldering as a fundamental combustion mechanism, but also support the development of a database to guide the optimal oxygen supply in solid waste management and evaluate the fire risk associated with smouldering.

4. Conclusions

In this work, we experimentally determined the role of fuel bulk density and particle size on the minimum oxygen supply for smouldering combustion. Pine needles with various bulk densities and wood samples with different particle sizes were chosen as typical porous fuels and the experiments were performed in a tubular smouldering reactor. After ignition at the middle of the fuel bed, the generated smouldering front was fed with a prescribed airflow. Generally, as the flow velocity decreases, three types of phenomena were observed, i.e., bidirectional propagation (forward and opposed), unidirectional propagation (opposed) and no propagation (extinction). The bidirectional propagating front is possibly due to (I) excessive oxygen supply that cannot be completely consumed by a single opposed front; (II) a non-uniform smouldering front, as a result of large particle size or low fuel bulk density cannot fully homogenizing the provided oxidizer.

Moreover, the minimum airflow velocity to sustain smouldering propagation increases as the bulk density decreases, or the fuel particle

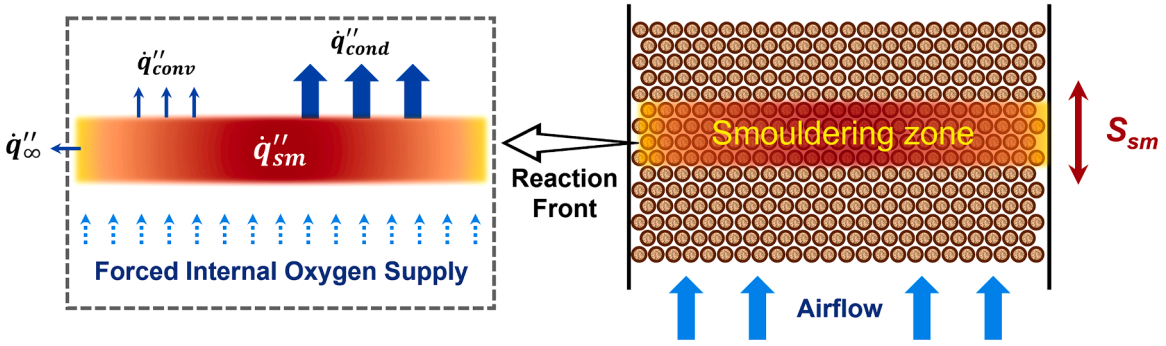

Fig. 10. Schematics for the energy balance for a propagating smouldering front at near-limit conditions.

size increases. As bulk density gradually decreases or fuel particle size increases, the boundaries of different propagation modes merge, and eventually only bidirectional propagation is possible due to the oxygen "leakage" from the non-uniform smouldering front with larger pores. Finally, a simplified heat transfer process is proposed to reveal the important role of radiation heat transfer across pores in affecting the oxygen supply limit of smouldering propagation over porous media. Future work will establish a physics-based multi-dimensional model to reveal the underlying mechanism of near-limit smouldering propagation under different flow conditions.

5. Novelty and significance statement

The path and rate of oxygen supply are crucial for the smouldering combustion. However, in the literature, most studies aiming to understand the oxygen threshold of smouldering were performed under quiescent ambient or with an external wind, which cannot completely isolate the oxygen diffusion from the ambient. This has resulted in different values of limiting oxygen concentration (LOC) found for the same fuel in various experiments.

Our custom-made tubular reactor could flow the oxidizer through the porous fuel to the smouldering front without an ambient oxygen supply, ensuring the ability to explore the real oxygen threshold of smouldering propagation and understand the effect of fuel density and particle size. We found that both smouldering propagation mode and threshold are sensitive to the fuel density and particle size, and the interparticle radiation heat transfer could significantly affect the oxygen supply limit of smouldering propagation over porous media.

CRediT authorship contribution statement

Yunzhu Qin: Investigation, Data curation, Writing – original draft, Formal analysis, Resources. **Yichao Zhang:** Formal analysis, Resources. **Yuying Chen:** Formal analysis, Resources. **Shaorun Lin:** Supervision, Methodology, Writing – original draft, Formal analysis, Resources. **Xinyan Huang:** Conceptualization, Supervision, Methodology, Writing – review & editing, Formal analysis, Funding acquisition.

Declaration of competing interest

The authors declare that they have no known competing financial interests or personal relationships that could have appeared to influence the work reported in this paper.

Acknowledgments

This research is funded by the National Natural Science Foundation of China (NSFC) No. 52322610 and RGC Hong Kong GRF Scheme No. 15221523.

Supplementary materials

Supplementary material associated with this article can be found, in the online version, at doi:10.1016/j.combustflame.2024.113292.

References

[1] G. Rein. Smoldering Combustion, Chapter 19 in: SFPE Handbook of Fire Protection Engineering, 5th Edition, Springer, 2016, pp. 581–603, https://doi.org/10.1007/978-1-4939-2565-0_19.
[2] T.J. Ohlemiller, Modeling of smoldering combustion propagation, Prog. Energy Combust. Sci. 11 (1985) 277–310.
[3] G. Rein, Smouldering fires and natural fuels, Fire Phenom. Earth Syst. An Interdiscip. Guid. to Fire Sci. (2013) 15–33.
[4] J.L. Torero, J.I. Gerhard, M.F. Martins, M.A.B. Zanoni, T.L. Rashwan, J.K. Brown, Processes defining smouldering combustion: integrated review and synthesis, Prog. Energy Combust. Sci. 81 (2020) 100869.
[5] T.J. Ohlemiller. Smoldering combustion, National Institute of Standards and Technology, Gaithersburg, MD, 1986.
[6] A. Anca-Couce, N. Zobel, A. Berger, F. Behrendt, Smouldering of pine wood: kinetics and reaction heats, Combust. Flame. 159 (2012) 1708–1719.
[7] R.S. Miller, J. Bellan, A generalized biomass pyrolysis model based on superimposed cellulose, hemicellulose and lignin kinetics, Combust. Sci. Technol. 126 (1997) 97–137.
[8] E. Villacorta, I. Haraldseid, R.F. Mikalsen, B.C. Hagen, S. Erland, G. Kleppe, U. Krause, V. Frette, Onset of smoldering fires in storage silos: susceptibility to design, scenario, and material parameters, Fuel 284 (2021) 118964.
[9] S. Lin, P. Sun, X. Huang, Can peat soil support a flaming wildfire? Int. J. Wildl. Fire. 28 (2019) 601–613.
[10] B. Berg, K. Hannus, T. Popoff, O. Theander, Changes in organic chemical components of needle litter during decomposition. Long-term decomposition in a Scots pine forest: i.(Pinus sylvestris), Can. J. Bot. 60 (1982) 1310–1319.
[11] K. Miyanishi. "Duff Consumption", Forest Fires: Behavior and Ecological Effects, Academic Press, 2001, pp. 437–475.
[12] Russell A. Ogle, S.E. Dillon, M. Fecke, Explosion from a smoldering silo fire, Process Saf. Prog. 33 (2013) 94–103.
[13] Z. Liang, S. Lin, X. Huang, Smoldering ignition and emission dynamics of wood under low irradiation, Fire Mater. 47 (2022) 514–524.
[14] G. Rein, X. Huang, Smouldering wildfires in peatlands, forests and the arctic: challenges and perspectives, Curr. Opin. Environ. Sci. Heal. 24 (2021) 100296.
[15] T.J. Ohlemiller, Smoldering combustion propagation on solid wood, Fire Saf. Sci. Proc. Third Int. Symp. (2006) 565–574.
[16] S. Wang, P. Ding, S. Lin, X. Huang, A. Usmani, Deformation of wood slice in fire: interactions between heterogeneous chemistry and thermomechanical stress, Proc. Combust. Inst. 38 (2021) 5081–5090.
[17] D. Wu, X. Huang, F. Norman, F. Verplaetsen, J. Berghmans, E. Van Den Bulck, Experimental investigation on the self-ignition behaviour of coal dust accumulations in oxy-fuel combustion system, Fuel 160 (2015) 245–254.
[18] Y. Chen, S. Lin, Z. Liang, X. Huang, Clean smoldering biowaste process: effect of burning direction on smoke purification by self-sustained flame, Fuel Process. Technol. 237 (2022) 107453.
[19] Z. Song, T. He, M. Li, D. Wu, F. You, Self-sustaining smoldering as a novel disposal approach for food waste with high moisture content, Fuel Process. Technol. 228 (2022) 107144.
[20] Y. Chen, S. Lin, Z. Liang, N.C. Surawski, X. Huang, Smouldering organic waste removal technology with smoke emissions cleaned by self-sustained flame, J. Clean. Prod. 362 (2022) 132363.
[21] Y. Qin, Y. Chen, S. Lin, X. Huang, Limiting oxygen concentration and supply rate of smoldering propagation, Combust. Flame 245 (2022) 112380.
[22] T.L. Rashwan, J.L. Torero, J.I. Gerhard, Heat losses in applied smouldering systems: sensitivity analysis via analytical modelling, Int. J. Heat Mass Transf. 172 (2021) 121150.
[23] S. Lin, T.H. Chow, X. Huang, Smoldering propagation and blow-off on consolidated fuel under external airflow, Combust. Flame. 234 (2021) 111685.
[24] F. Richter, F.X. Jervis, X. Huang, G. Rein, Effect of oxygen on the burning rate of wood, Combust. Flame. 234 (2021) 111591.
[25] Y. Qin, D. Nur, S. Musa, S. Lin, X. Huang, Deep peat fire persistently smouldering for weeks : a laboratory demonstration, Int. J. Wildl. Fire 32 (2022) 86–98.
[26] G. B.Starcher, A. Prakash, E. V.Sokol, Coal and Peat Fires:A Global Perspective, 1st ed., Elsevier, Oxford, 2011.
[27] X. Huang, G. Rein, Interactions of Earth's atmospheric oxygen and fuel moisture in smouldering wildfires, Sci. Total Environ. 572 (2016) 1440–1446.
[28] C.M. Belcher, J.M. Yearsley, R.M. Hadden, J.C. Mcelwain, G. Rein, Baseline intrinsic flammability of Earth ' s ecosystems estimated from paleoatmospheric oxygen over the past 350 million years, Proc. Natl. Acad. Sci. 107 (2010) 22448–22453.
[29] R.M. Hadden, G. Rein, C.M. Belcher, Study of the competing chemical reactions in the initiation and spread of smouldering combustion in peat, Proc. Combust. Inst. 34 (2013) 2547–2553.
[30] A. Ronda, M.Della Zassa, A. Biasin, M.A. Martin-Lara, P. Canu, Experimental investigation on the smouldering of pine bark, Fuel 193 (2017) 81–94.
[31] R. Hadden, G. Rein, Chapter 18 - Burning and Water Suppression of Smoldering Coal Fires in Small-Scale Laboratory Experiments. Coal and Peat Fires: A Global Perspective, Elsevier, Amsterdam, 2011, pp. 317–326.
[32] L. Yermán, R.M. Hadden, J. Carrascal, I. Fabris, D. Cormier, J.L. Torero, J. I. Gerhard, M. Krajcovic, P. Pironi, Y.-L. Cheng, Smouldering combustion as a treatment technology for faeces: exploring the parameter space, Fuel 147 (2015) 108–116.
[33] I. Fabris, D. Cormier, J.I. Gerhard, T. Bartczak, M. Kortschot, J.L. Torero, Y.-L. Cheng, Continuous, self-sustaining smouldering destruction of simulated faeces, Fuel 190 (2017) 58–66.
[34] X. Huang, J. Gao, A review of near-limit opposed fire spread, Fire Saf. J. 120 (2021) 103141.
[35] H. Zhang, Y. Qiao, H. Chen, N. Liu, L. Zhang, X. Xie, Experimental study on flaming ignition of pine needles by simulated lightning discharge, Fire Saf. J. 120 (2021) 103029.
[36] R.J. Yokelson, D.W.T. Griffith, D.E. Ward, Open-path fourier transform infrared studies of large-scale laboratory biomass fires, J. Geophys. Res. Atmos. 101 (1996) 21067–21080.
[37] Y. Hu, E.G. Christensen, H.M.F. Amin, T.E.L. Smith, G. Rein, Experimental study of moisture content effects on the transient gas and particle emissions from peat fires, Combust. Flame. 209 (2019) 408–417.

[38] S. Lin, X. Huang, Quenching of smoldering: effect of wall cooling on extinction, Proc. Combust. Inst. 38 (2021) 5015–5022.
[39] S. Lin, H. Yuan, X. Huang, A computational study on the quenching and near-limit propagation of smoldering combustion, Combust. Flame. 238 (2022) 111937.
[40] A. Bar-Ilan, G. Rein, D.C. Walther, A.C. Fernandez-Pello, J.L. Torero, D.L. Urban, The effect of buoyancy on opposed smoldering, Combust. Sci. Technol. 176 (2004) 2027–2055.
[41] T.L. Rashwan, J.L. Torero, J.I. Gerhard, Heat losses in a smouldering system: the key role of non-uniform air flux, Combust. Flame. 227 (2021) 309–321.
[42] J.L. Torero, A.C. Fernandez-Pello, Forward smolder of polyurethane foam in a forced air flow, Combust. Flame. 106 (1996) 89–109.
[43] C. Lautenberger, C. Fernandez-Pello, Generalized pyrolysis model for combustible solids, Fire Saf. J. 44 (2009) 819–839.
[44] X. Huang, G. Rein, Thermochemical conversion of biomass in smouldering combustion across scales: the roles of heterogeneous kinetics, oxygen and transport phenomena, Bioresour. Technol. 207 (2016) 409–421.
[45] F. Yu, G. Wei, X. Zhang, K. Chen, Two effective thermal conductivity models for porous media with hollow spherical agglomerates, Int. J. Thermophys. 27 (2006) 293–303.